Seasonal transition of SST anomalies in the tropical Indian Ocean during El Niño and Indian Ocean Dipole years

Hiroki Tokinaga and Youichi Tanimoto

Graduate School of Environmental Earth Science, Hokkaido University

Sapporo 060-0810, Japan

(*Manuscript received 23 January 2003, in final form 20 March 2004*)

Journal of the Meteorological Society of Japan

Corresponding author address: Hiroki Tokinaga,
Graduate School of Environmental Earth Science, Hokkaido University
N10W5, Kita-ku, Sapporo, 060-0810, Japan
E-mail: tokinaga@ees.hokudai.ac.jp

ABSTRACT

We investigated seasonal transition of dominant modes of sea surface temperature anomalies (SSTAs) in the tropical Indian Ocean, analyzing the National Centers for Environmental Prediction/National Center for Atmospheric Research reanalysis products (NCEP/NCAR reanalyses), the Global sea-Ice and SST dataset (GISST2.3b), and the Simple Ocean Data Assimilation (SODA). During the coincidence years when the Indian Ocean Dipole (IOD) is followed by the major El Niño during boreal autumn-winter season, surface dipole structure in the tropical Indian Ocean tends to turn into the basinwide warm pattern in the November-December period. In contrast, the subsurface dipole keeps its structure from boreal autumn to winter. Such a surface-confined transition of SSTA is induced by latent heat flux anomalies in the eastern Indian Ocean. These latent heat flux anomalies are associated with changes in scalar wind speed anomalies. The zonal direction of climatological surface winds changes from easterly into westerly over the eastern Indian Ocean in November-December, while the anomalous Walker circulation during the El Niño induces easterly surface wind anomalies to persist there. As a result, a deceleration of scalar wind speed takes place during boreal winter, and leads to warming of SST through suppressed evaporation. In addition to these latent heat flux anomalies, incoming solar radiation anomalies contribute to the net surface warming during this period. Furthermore, we discuss the role of the ocean dynamics for keeping the warm SSTAs in the western Indian Ocean.

1. Introduction

The previous observational studies for sea surface temperature anomalies (SSTAs) in the Indian Ocean (Tourre and White 1995; Chambers et al. 1999; Saji et al. 1999; Dommenget and Latif 2002) identified two dominant spatial structures from an empirical orthogonal function (EOF) analysis. Those leading EOFs, which accounts for 30-40 % of the total variance, represent a basinwide pattern with uniform polarity. The accompanying time series (principal components; PCs) of this mode tend to exceed one standard deviation during the boreal winter-spring season. In addition, these PCs are strongly correlated with the Niño3 area-averaged SSTA index, which indicates that this basinwide warm/cold pattern of SSTA is concurrent with the major El Niño/La Niña event (Tourre and White 1995; Chambers et al. 1999; Klein et al. 1999). During a mature season (December-March) of the El Niño, convective activity is suppressed over the region from the eastern Indian Ocean to western Pacific. Venzke et al.'s (2000) experiments, with the coupled ocean-atmosphere general circulation model (CGCM), showed that this suppressed convection associated with the El Niño increases the effective solar radiation over the eastern Indian Ocean, which increases the underlying SST. They also indicated that latent heat flux plays an important role in warming SST in the western and central Indian Ocean, where wind speed is strongly influenced by the anomalous Walker circulation. Thus, the lower-atmospheric conditions are modulated by the El Niño, and cause the basinwide warm pattern of boreal winter-spring SSTA in the tropical Indian Ocean.

The second EOF, which accounts for about 10 %, has attracted great attention in recent years as a zonal SST dipole structure (Saji et al. 1999; Webster et al. 1999; Murtugudde et al. 2000). This zonal SST dipole is most dominant in boreal autumn with its PCs exceeding one standard deviation. During this season, regressed surface wind anomalies onto the PCs represent easterlies and southeasterlies off the west coast of Sumatra Island, which induce upwelling and evaporative cooling of SST in the eastern Indian Ocean (Behera et al. 1999; Saji et al. 1999; Vinayachandran et al. 1999; Ueda and Matsumoto 2000). In addition, these anomalous surface easterlies force a westward downwelling Rossby wave

and deepen thermocline (suppression of upwelling) in the western Indian Ocean (Chambers et al. 1999; Webster et al. 1999; Murtugudde et al. 2000; Xie et al. 2002). These processes during boreal autumn lead to the positive phase of zonal SST dipole; positive (negative) SSTAs in the western (eastern) Indian Ocean.

However, the origin of this zonal SST dipole has been controversial among the previous studies. This controversy seems to arise from a difference on the treatment of statistical analyses between their approaches. Saji et al. (1999) and Webster et al. (1999) indicated that the zonal SST dipole is not influenced by the ENSO in the Pacific, because of insignificant correlation coefficient (r=0.35) between the zonal SST dipole index and Niño3 SSTA time series calculated from 12 months $\times$ 41 years = 492 samples. Therefore, these studies concluded that internal dynamics confined in the Indian Ocean is responsible for the zonal SST dipole.

In contrast, some of the positive zonal SST dipoles coincide with the major El Niño events, which appear in 1963, 1972, 1982, and 1997. Several statistical studies (Allan et al. 2001; Baquero-Bernal et al. 2002) have shown a significant correlation coefficient (r=0.56) between the zonal SST dipole and Niño3 SST indices calculated from September-November mean anomalies (1 season $\times$ 40 years = 40 samples), while the correlation coefficients in the other seasons are insignificant. Using only boreal-autumn means, the regressed SSTAs and surface wind anomalies onto the Niño3-SSTA index represent the zonal SST dipole in the Indian Ocean and southeasterly along the Sumatra coast, respectively (Xie et al. 2002).

The previous studies (Saji et al. 1999; Ueda 2001; Allan et al. 2001; Baquero-Bernal et al. 2002) revealed that the appearance of the zonal SST dipole and basinwide warm pattern in the Indian Ocean depends on the season. Since these studies tend to focus on either zonal SST dipole or basinwide warm pattern independently, the seasonal sequence of the Indian Ocean SSTAs during the major El Niño years has not been investigated.

In this study, we describe the processes of seasonal transition of SSTAs in the tropical Indian Ocean. Section 2 briefly describes the datasets used in this study. In section 3,

we focus on the positive phase of zonal SST dipole concurrent with the major El Niño, and examine its association with the basinwide warm pattern of SSTA. This section also illustrates how the Indian Ocean makes seasonal progress in SSTA during the major El Niño years. In section 4, we examine the lower-atmospheric processes which induce the transition of the boreal-autumn zonal SST dipole into the boreal-winter basinwide warm pattern. Section 5 summarizes this study.

2. Data

Atmospheric variables in this study are monthly horizontal wind velocity, vertical velocity, and surface heat fluxes in the National Centers for Environmental Prediction/National Center for Atmospheric Research reanalysis products (NCEP/NCAR reanalyses; Kalnay et al. 1996) from 1948 to 1999. The spatial resolution of the NCEP/NCAR reanalyses is horizontally 2.5° latitude-longitude and vertically 12 levels (1000, 925, 850, 700, 600, 500, 400, 300, 250, 200, 150, and 100 hPa).

SST data is the Global sea-ice and SST data 2.3b (GISST2.3b; Parker et al. 1995) from 1948 to 1999. The GISST2.3b has monthly 1° latitude-longitude resolution. In addition to SST, we analyze monthly upper-ocean temperatures in the Simple Ocean Data Assimilation (SODA; Carton et al. 2000a, b) from 1950 to 1999. The SODA has 20 vertical levels with 15-m resolution near the sea surface, and is available at 0.45°× 1° latitude-longitude in the tropics (4°S $\sim$ 4°N) and 1° latitude-longitude in the extratropics.

We also use the Dipole Mode Index (DMI) by Saji et al. (1999) and Niño3-SSTA index (NINO3) to identify the years when the Indian Ocean Dipole (IOD) and ENSO simultaneously occurred. The DMI is defined as a difference of area-averaged SSTA between the western (50-70°E, 10°S-10°N) and eastern (90-110°E, 10°S-0) Indian Ocean, and the NINO3 is a SST anomaly averaged in the equatorial eastern Pacific (150-90°W, 5°S-5°N).

To extract the variation with the timescale for the typical ENSO and IOD, the variability with period of 7 years and longer has been removed from these datasets by using harmonic analysis.

3. Ocean-Atmosphere variability over the Indo-Pacific sector

a. Zonal SST dipole, basinwide warm pattern and El Niño

Figure 1 shows a scatter plot of the boreal autumn (September-November) DMI and NINO3. The positive (negative) phase of IOD over one standard deviation occurred nine (four) times in the past 52 years. During several positive events of IOD, the major El Niño appears in the tropical Pacific (1963, 1972, 1982, 1986, 1997; hereafter refer to the 'coincidence years'). This coincidence of the positive IODs and major El Niño events contributes to significant correlation coefficient between the two indices (+0.6). **Fig. 1.**

We make composite maps of SST and surface wind anomalies during the coincidence years (Fig. 2). During the June-August period (Fig. 2a), the warm tongue structure of SSTA appears east of 170°E in the tropical Pacific, and surface westerly wind anomalies prevails over the tropical western Pacific. Meanwhile, southeasterly wind anomalies off the west coast of Sumatra Island appear along the weak SST anomaly gradient from the southeastern to western Indian Ocean. During the September-November period (Fig. 2b), the warm tongue structure of SSTA and westerly wind anomalies are further enhanced over the tropical Pacific. At the same time, the easterly and southeasterly wind anomalies prevail over the eastern Indian Ocean, and a zonal dipole of SSTA becomes more apparent in the tropical Indian Ocean. In the following December-February period (Fig. 2c), SSTAs and surface wind anomalies in the tropical Pacific keep the conspicuous structure associated with the El Niño. In the Indian Ocean, a basinwide warm pattern appears instead of the zonal SST dipole, despite the fact that the strength of easterly wind anomalies unchanges over the eastern Indian Ocean. Although the basinwide warm pattern arises in the other El Niño years (1957, 1965, 1969, 1976, 1987) without strong IODs, it has much smaller amplitudes of SSTA than in the coincident years (not shown). **Fig. 2.**

Also in the incoincidence years (1961, 1967, 1977, 1994) when positive IODs occur without El Niño events, the zonal dipole structure of SSTA in the Indian Ocean is prominent during the September-November period (Fig. 3b). The associated SSTA and surface wind anomaly patterns during this season are quite similar to those in the coincidence years **Fig. 3.**

(Fig. 2b) except for the SSTA amplitudes in the southeastern Indian Ocean. However, the basinwide warm pattern does not appear during the following December-February period in the incoincidence years (Fig. 3c). These findings indicate that a remote forcing from the SST activity in the tropical eastern Pacific is relevant to the seasonal transition of SSTAs in the tropical Indian Ocean.

The zonal SST dipole and basinwide warm pattern are identified as the leading EOF for September-October-November and December-January-February mean SST anomalies in the tropical Indian Ocean, respectively. Figure 4 shows the two accompanying PCs calculated from loadings in the Indian Ocean, and regressed SSTAs onto the PCs. The most striking feature of the boreal autumn EOF, which accounts for 31.9 % of total variance on interannual timescale, is the zonal dipole structure. This spatial structure is quite similar to that of the zonal SST dipole in the coincidence years (Fig. 2b).

Fig. 4.

The leading EOF for boreal winter SSTAs, which accounts for 38.5 % of total variance, has single polarity over most of the domain with centers of action in the western half of the southern tropical Indian Ocean and south of 20°S in the eastern portion of the basin (Fig. 4b). This spatial structure is quite similar to the basinwide warm pattern of SSTAs in the coincidence years (Fig. 2c). Although these EOFs are derived from different seasons, a significant correlation (+0.67) between the two PCs indicates a temporal linkage between the zonal SST dipole in boreal autumn and the basinwide warm pattern in boreal winter (Fig. 4c). In addition, each of the two PCs shows significant values exceeding one standard deviation during the major El Niño years. The same relationship between the zonal SST dipole and basinwide warm pattern can be detected from the leading mode of the singular value decomposition (SVD) analysis for the boreal autumn and winter SSTAs in the Indian Ocean (not shown).

b. Surface and subsurface temperature variations

In order to examine the seasonal sequence that the boreal-autumn zonal SST dipole turns into the boreal-winter basinwide warm pattern, we present a longitude-depth section of composite anomalies of zonal and vertical wind velocity, SST, and subsurface temperature

Fig. 5.

averaged over 5°S and 5°N during the coincidence years (Fig. 5). In July (Fig. 5a), negative anomalies of SST and subsurface temperature are found in the eastern Indian Ocean and the western Pacific. Strong negative temperature anomalies at the climatological thermocline depth of 100 meters indicates that surface southeasterly wind anomalies over the eastern Indian Ocean lead to upwelling of cold water off the west coast of Sumatra Island (Fig. 2a). The zonal SST dipole, however, does not become apparent at the surface and subsurface in this period. At the same time, positive SSTAs are still outcroped east of the dateline in the equatorial Pacific. Underlying subsurface anomalies along tilted thermocline are much coherent, which seems the pre-condition of the boreal-winter mature phase of El Niño. The associated change in the tropospheric cross section shows a pronounced baroclinic structure over the Pacific sector, while no coherent cell appears outside the Pacific.

In October (Fig. 5b), downward anomalies over the region east of the maritime continent become much stronger, which is associated with anomalous surface westerlies (easterlies) over the western and central Pacific (the Indian Ocean), as seen in Fig. 2b. A coherent dipole structure of temperature anomalies is found from the surface to 200 meters depth in the Indian Ocean. East of downward wind anomalies over the western Pacific, positive temperature anomalies at surface (subsurface) are intensified east of 160°E (160°W). Therefore, the convective activities are strongly suppressed over the maritime continent. In the following January (Fig. 5c), strength of the two cells over the Indo-Pacific sector persists, and center of downward wind anomalies moves eastward. In the Indian Ocean, a surface structure shows a drastic change from the zonal dipole into the basinwide warm pattern, despite the fact that the subsurface dipole is still found between 50 - 150 meters.

Figure 6 shows two monthly time series of zonal temperature differences in the surface and subsurface, DMI_{SST} and DMI_{100m}. This figure presents a seasonal sequence of zonal dipole structure during the coincidence years. From May to November, the two DMIs display synchronous development due to the intensification of the upwelling off the west coast of Sumatra Island. After the mature phase of each dipole, however, DMI_{SST} decreases more rapidly than DMI_{100m}. While DMI_{SST} is close to zero in the following January and

Fig. 6.

becomes negative for four months after that, DMI_{100m} remains positive to the following May though a gradual decrease of its amplitude. After boreal autumn in the coincidence years, positive temperature anomalies in the southeastern Indian Ocean are confined in the upper 40m of the ocean. This suggests that the warming effect due to surface heat fluxes appears only in the oceanic mixed layer. We shall discuss this further in the next section.

4. Surface heat fluxes

Fig. 7.

Figure 7a displays the composite anomalies of the oceanic mixed layer temperature (T_{MLD}) and surface heat fluxes averaged over the eastern part of the zonal SST dipole (90°-110°E, 10°S-0°; the southeastern Indian Ocean) during the coincidence years. The positive (negative) value of surface heat fluxes means downward (upward) anomaly. In this study, the oceanic mixed layer depth (MLD) is defined to be the depth at which the temperature differs from the surface value by greater than 0.8 ℃. The net surface heat flux anomaly, which is mostly explained by latent heat flux, shows a cooling effect on T_{MLD} from July through October. This net surface heat flux anomaly is consistent with T_{MLD} tendency in the same region. After that season, the net surface heat flux anomaly shows a warming effect on T_{MLD} from December to the following February, despite the fact that autumn-winter anomalies of surface wind velocity keep its direction to the west. This increase in T_{MLD} is associated with suppressed latent heat flux during the same period. The solar radiation anomaly keeps warming the oceanic mixed layer from June to the following February due to the suppression of convective activity over the maritime continent (Fig. 5). Thus, the net heat flux turns into warming effect during October-November, which is two months earlier than a polarity change in latent heat flux anomaly. The time series of T_{MLD} anomaly lags by 2-3 months behind the net surface heat flux anomaly, and switches its polarity during November to December. This shift of T_{MLD} polarity coincides with the transition of the zonal SST dipole into the basinwide warm pattern in Figs. 2 and 5.

Figure 7b shows the composite and climatology of the MLD in the eastern part of the zonal SST dipole. The climatological MLD is characterized by an annual cycle in which the

MLD is deepest ($\sim$ 60m) in August and shallowest ($\sim$ 30m) in April. The composite MLD also indicates similar annual cycle to the climatological one. Since the MLD in the south-eastern Indian Ocean tends to be shallower from boreal summer to the following spring, the contribution of surface heat flux to the T_{MLD} change becomes increasingly larger even if the input of surface heat flux is constant through the season. In addition, the composite MLD is shallower than the climatological one, because the anomalous southwesterlies off the west coast of Sumatra Island intensify upwelling of cold water and thereby raise the thermocline depth. From Figs. 7a and 7b, the averaged net heat flux and MLD during the warming period (from November to the following February) are about 15 W m^{-2} and 35 m, respectively. This MLD agrees with the depth of the upper layer in which the positive temperature anomalies appears after the mature phase of the zonal SST dipole (Fig. 5). If the upper 35 m of the ocean is warmed up by the heat input due to this flux, we can estimate the T_{MLD} change for 3 months to be about 0.8 ℃, using the following equation:

$$\frac{\partial T_{MLD}}{\partial t} = \frac{F}{C_p \rho H}$$

where t is time, F is the heat flux into the ocean, C_p is specific heat of water (4218 $JK^{-1}kg^{-1}$), ρ is density of water (1000 kgm^{-3}), and H is oceanic mixed layer depth. This value of 0.8 ℃ accounts for about 70 % of the T_{MLD} change during the warming period.

To examine the shift of T_{MLD} polarity associated with the seasonal change in the latent heat flux anomaly during the warming period, we present the climatological zonal wind at surface together with its composite anomaly of zonal wind in Fig. 7c. The climatological zonal wind shows an obvious annual cycle of monsoon system that is characterized by easterly (westerly) wind from April (December) to November (the following March). On the other hand, the anomalous Walker circulation associated with the El Niño induces surface easterly wind anomaly all the year around. This easterly wind anomaly accelerates (decelerates) the climatological easterly (westerly) wind from April (December) to November (March). Consequently, the negative anomaly of zonal wind induces positive (negative) scalar wind speed anomaly, and thereby leads to an enhanced (suppressed) evaporative

cooling during boreal autumn (winter), as suggested by Ueda and Matsumoto (2000) and Ueda (2001). This seasonal change in latent heat flux anomaly induces the rapid decay of the zonal SST dipole.

Figure 8 shows the composite anomalies of T_{MLD} and surface heat fluxes averaged over the western part of the zonal SST dipole (50°-70°E, 10°S-10°N) for the coincidence years. The positive T_{MLD} anomaly, with its maximum in November, is dominant all the year around. On the other hand, the surface heat fluxes shows a cooling effect on T_{MLD}. In other words, the T_{MLD} in this region is not determined only by an atmospheric forcing during boreal winter-spring season. Although Venzke et al. (2000) indicated from CGCM integrations that latent heat fluxes play an active role in SST warming in the western Indian Ocean, the result in this study implies that an ocean dynamics contributes to the change of T_{MLD} there, as demonstrated by the previous studies (Webster et al. 1999; Chambers et al. 1999; Xie et al. 2002).

Fig. 8.

5. Conclusion

We have studied the seasonality of the Indian Ocean SST anomalies associated with the El Niño and IOD, using several model-based assimilation products. In the tropical Indian Ocean, there are two dominant structures of SSTAs on interannual timescale. One is a zonal dipole in boreal autumn, which is characterized by anomalous cold (warm) SSTAs in the southeastern (western) Indian Ocean, and the other is a basinwide warm/cold pattern during boreal winter-spring season. Thus, the dominant structure of the Indian Ocean SST strongly depends on the season.

When the El Niño and IOD simultaneously take place in the Indo-Pacific sector, the boreal-autumn zonal SST dipole turns into the boreal-winter basinwide warm pattern (Figs. 2 and 5), despite the fact that a zonal subsurface dipole lasts 3 months after the disappearance of the zonal SST dipole (Fig. 6). The El Niño suppresses the convective activities around the maritime continent from boreal summer to winter, which induces divergent wind anomalies in the lower troposphere (Fig. 5). Over the southeastern Indian

Ocean, the resultant surface easterly anomalies accelerate the climatological surface easterlies from boreal summer to autumn. Increases in alongshore component of surface wind lead to SST cooling through evaporation and upwelling in the southeastern Indian Ocean.

After boreal autumn, however, the SST cooling in the southeastern Indian Ocean is prevented through suppression of upward latent heat fluxes. The easterly wind anomalies are persistent due to the anomalous surface divergence over the maritime continent. These easterly wind anomalies decelerate the climatological westerly winds that are dominant during boreal winter to the following spring. In addition, the suppression of convective activity increases solar radiations over the southeastern Indian Ocean, which are partly responsible for warming tendency of SSTA during boreal winter and the following spring in the same region. Besides these heat flux input, the MLD during the coincidence years is shallower than the climatological MLD due to the anomalous upwelling off the west coast of Sumatra Island. These conditions are favorable for the appearance of the basinwide warm pattern and thereby induce the rapid decay of the zonal SST dipole. Although this SST warming occurs through the same mechanism in the minor El Niño years without the IOD, the SSTA amplitude in the Indian Ocean is smaller than a half of that in the coincident years (not shown). On the other hand, positive SSTAs in the western Indian Ocean persist from boreal autumn to the following spring despite a cooling effect of surface heat fluxes. This indicates that an ocean dynamics plays a significant role in the persistence of warm SSTAs in the western Indian Ocean during boreal winter-spring season. Our results show that the relationships between the anomalous zonal wind and the climatological wind over the southeastern Indian Ocean are different between boreal autumn and winter-spring season. This change in relationship is a key to link the zonal SST dipole and the basinwide warm pattern of SSTAs in the tropical Indian Ocean.

Acknowledgments

We express special thanks to Profs. M. Ikeda, K. Yamazaki, A. Kubokawa and S. -P. Xie for their helpful discussions and suggestions. The manuscript benefitted from the

constructive comments by the anonymous reviewers. This work was partially supported by Grand-In-Aid for Scientific Research defrayed by the Ministry of Education, Culture, Sports, Science and Technology of Japan (15540416). All figures were generated using the Generic Mapping Tools (GMT).

References

Allan, R., D. Chambers, W. Drosdowsky, H. Hendon, M. Latif, N. Nicholls, I. Smith, R. Stone, and Y. Tourre, 2001: Is there an Indian Ocean dipole, and is it independent of the El Niño-Southern Oscillation ? *CLIVER Exch.*, **6**, 18–22.

Baquero-Bernal, A., M. Latif, and S. Legutke, 2002: On dipolelike variability of sea surface temperature in the tropical Indian Ocean. *J. Climate*, **15**, 1358–1368.

Behera, S. K., R. Krishnan, and T. Yamagata, 1999: Unusual ocean-atmosphere conditions in the tropical Indian Ocean during 1994. *Geophys. Res. Lett.*, **26**, 3001–3004.

Carton, J. A., G. Chepurin, X. Cao, and B. Giese, 2000a: A simple ocean data assimilation analysis of the global upper ocean 1950-95. Part I: Methodology. *J. Phys. Oceanogr.*, **30**, 294–309.

——, ——, and ——, 2000b: A simple ocean data assimilation analysis of the global upper ocean 1950-95. Part Ⅱ: Results. *J. Phys. Oceanogr.*, **30**, 311–326.

Chambers, D. P., B. D. Tapley, and R. H. Stewart, 1999: Anomalous warming in the Indian Ocean coincident with El Niño. *J. Geophys. Res.*, **104**, 3035–3047.

Dommenget, D., and M. Latif, 2002: A caoutionary note on the interpretation of EOFs. *J. Climate*, **15**, 216–225.

Kalnay, E., M. Kanamitsu, R. Kistler, W. Collins, D. Deaven, L. Gandin, M. Iredell, S. Saha, G. White, J. Woollen, Y. Zhu, M. Chelliah, W. Ebisuzaki, W. Higgins, J. Janowiak, K. C. Mo, C. Ropelewski, J. Wang, A. Leetmaa, R. Reynolds, R. Jenne, and D. Joseph, 1996: The NCEP/NCAR 40-year reanalysis project. *Bull. Amer. Meteor. Soc.*, **77**, 437–471.

Klein, S. A., B. J. Soden, and N. C. Lau, 1999: Remote sea surface temperature variations during ENSO: Evidence for a tropical atmospheric bridge. *J. Climate*, **12**, 917–932.

Murtugudde, R., J. P. McCreary, and A. J. Busalacchi, 2000: Oceanic processes associated with anomalous events in the Indian Ocean with relevance to 1997-98. *J. Geophys. Res.*, **105**, 3295–3306.

Parker, D. E., C. K. Folland, and M. Jackson, 1995: Marine surface temperature: Observed variations and data requirements. *Climatic Change*, **31**, 559–600.

Saji, N. H., B. N. Goswami, P. N. Vinayachandran, and T. Yamagata, 1999: A dipole mode in the tropical Indian Ocean. *Nature*, **401**, 360–363.

Tourre, Y. M., and W. B. White, 1995: ENSO signals in global upper-ocean temperature. *J. Phys. Oceanogr.*, **25**, 1317–1332.

Ueda, H., 2001: Equatorial monsoon system as regulation for a dipole mode in the Indian Ocean. *Pap. Met. Geophys.*, **51**, 147–154.

——, and J. Matsumoto, 2000: A possible triggering process of east-west asymmetric anomalies over the Indian Ocean in relation to 1997/98 El Niño. *J. Meteor. Soc. Japan*, **78**, 803–818.

Venzke, S., M. Latif, and A. Villwock, 2000: The coupled GCM ECHO-2. Part Ⅱ: Indian Ocean response to ENSO. *J. Climate*, **13**, 1371–1383.

Vinayachandran, P. N., N. H. Saji, and T. Yamagata, 1999: Response of the equatorial Indian Ocean to an unusual wind event during 1994. *Geophys. Res. Lett.*, **26**, 1613–1617.

Webster, P. J., A. M. Moore, J. P. Loschnigg, and R. R. Leben, 1999: Coupled ocean-atmosphere dynamics in the Indian Ocean during 1997-98. *Nature*, **401**, 356–360.

Xie, S. P., H. Annamalai, F. A. Schott, and J. P. McCreary, 2002: Structure and mechanisms of south Indian Ocean climate variability. *J. Climate*, **15**, 864–878.

Captions of Figures

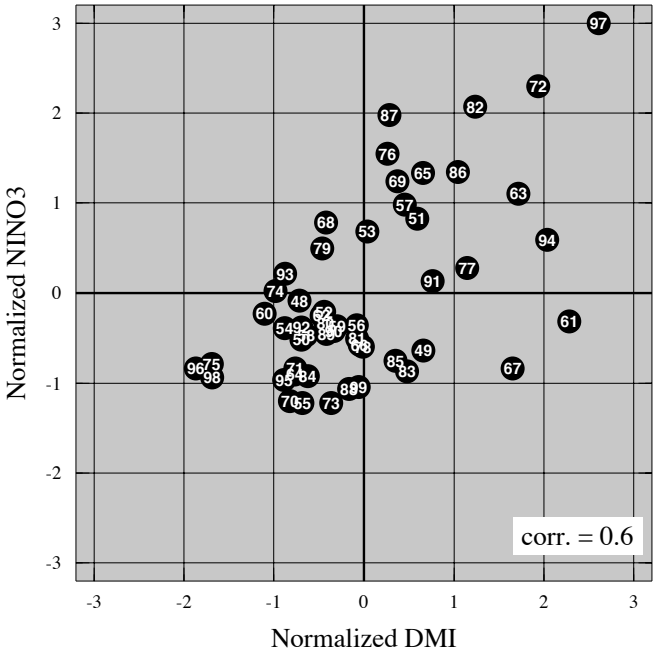

FIG. 1. The scatter plot of the normalized DMI and NINO3 calculated from September-October-November mean SST data. The number of two digits in the circle shows the last two ones of year from 1948 to 1999. The correlation coefficient between the two indices is +0.6.

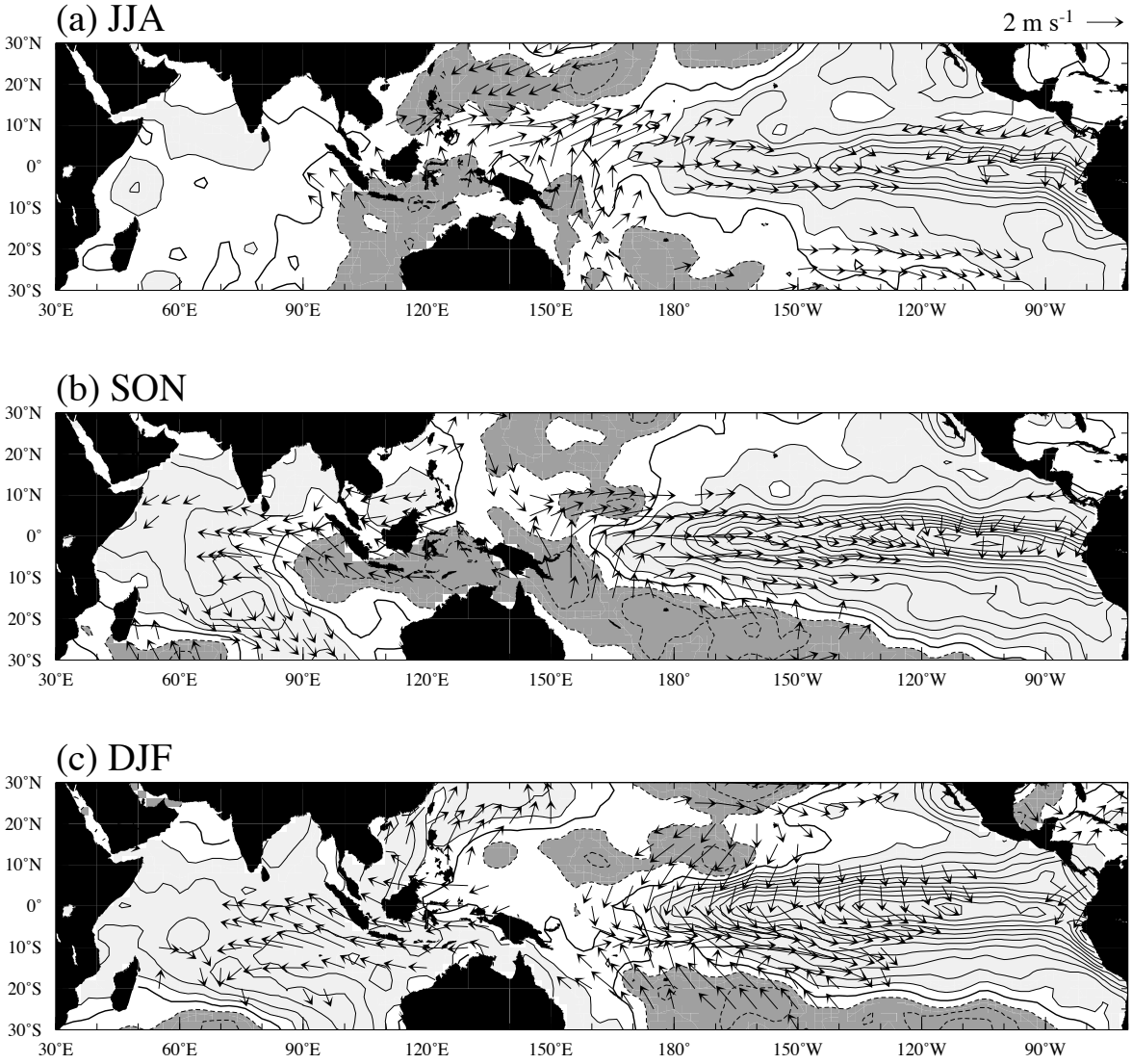

FIG. 2. The composite SST and surface wind anomalies averaged during (a) June to August (JJA), (b) September to November (SON), and (c) December to the following January (DJF) for the coincidence years (1963, 72, 82, 86, 97). In these years, the Indian Ocean Dipole and the El Niño simultaneously occurred. SST anomaly is represented by contour lines at 0.2 ℃ intervals. SST anomalies greater (less) than 0.2 (-0.2) ℃ are lightly (heavily) shaded. The reference wind speed (2 m s^{-1}) is indicated at the upper right corner of panels.

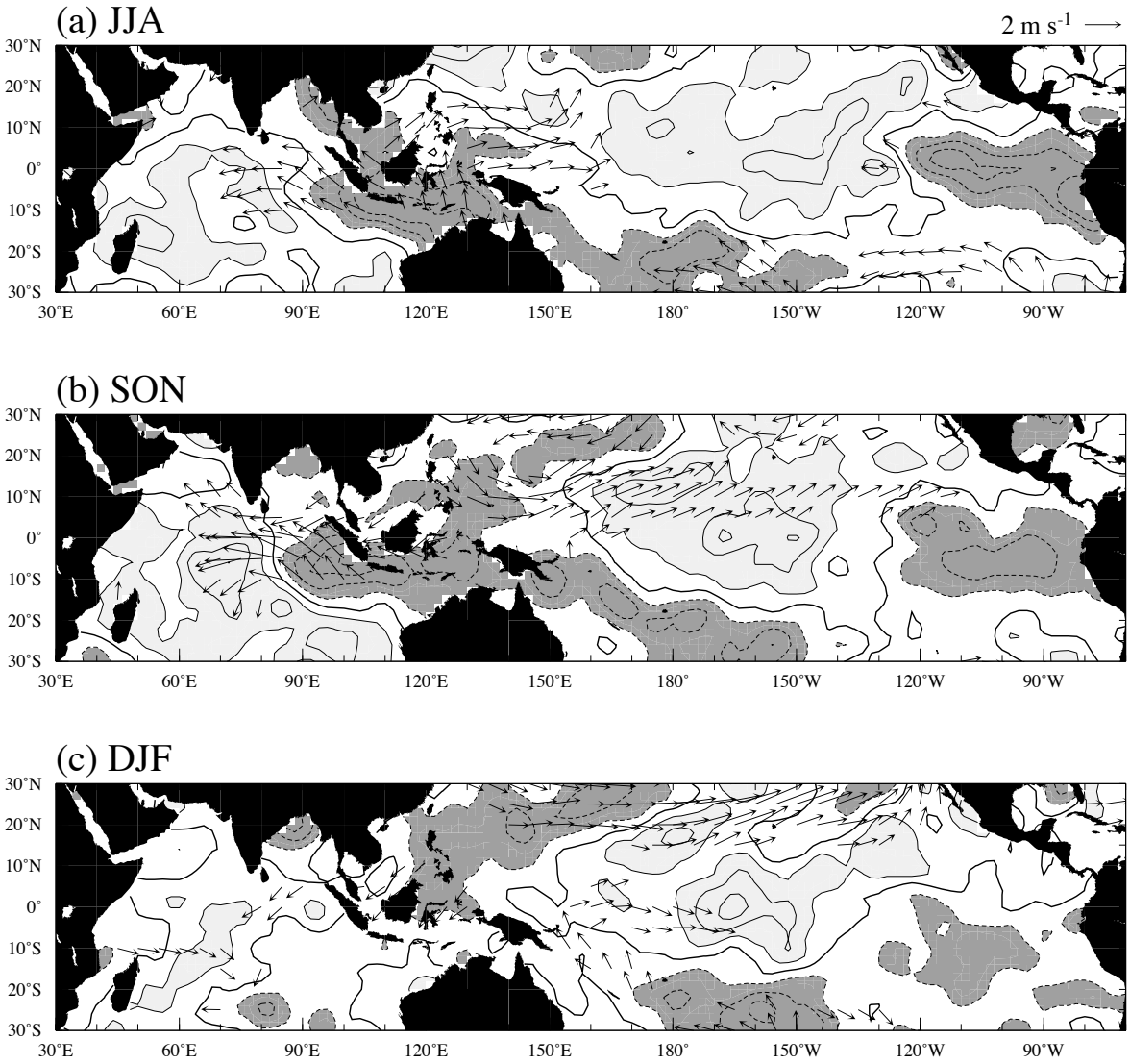

FIG. 3. Same as in Fig. 2, but for the incoincidence years (1961, 67, 77, 94) when the Indian Ocean SST dipole occurred in the non El Niño years.

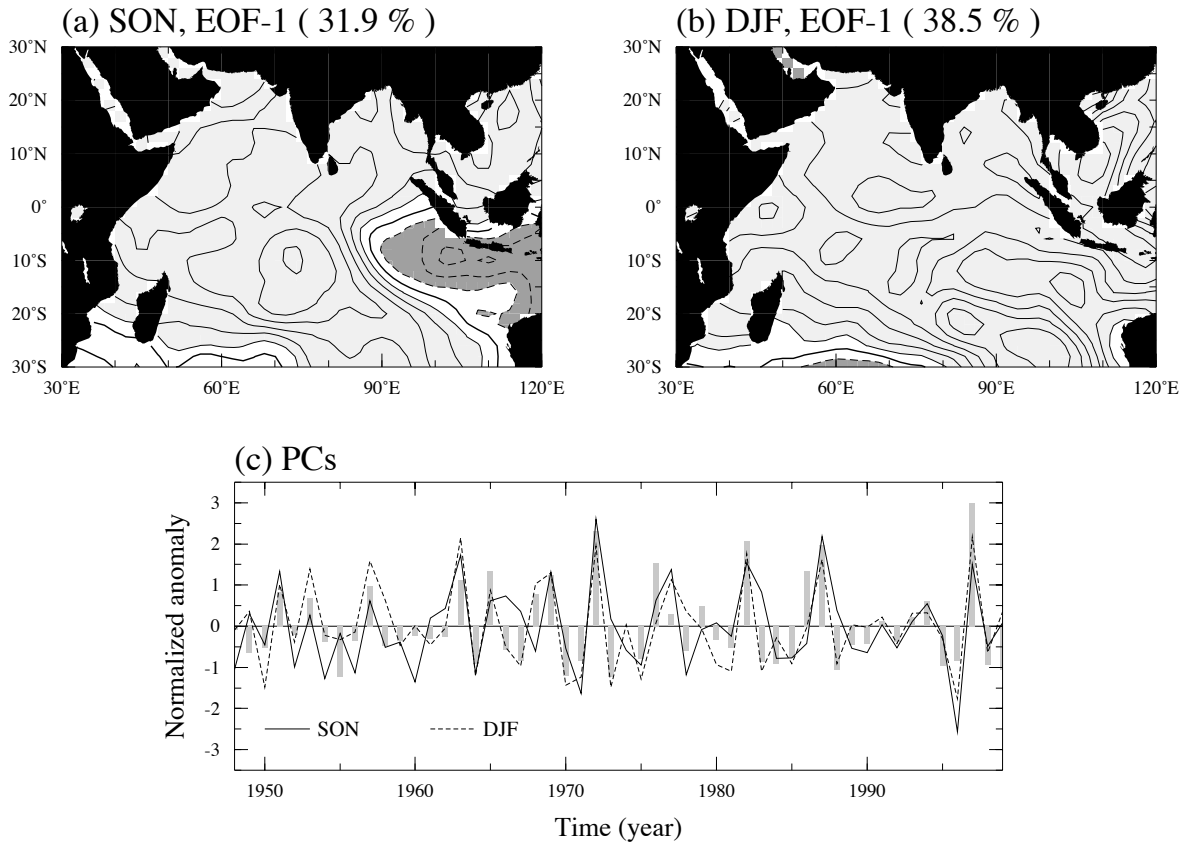

FIG. 4. The leading EOF modes for seasonal mean SST anomalies during (a) September-October-November (SON) and (b) December-January-February (DJF) in the Indian Ocean, respectively. The percentage of variance explained on the interannual timescale is indicated in the upper part at each panel. Contour lines show the regressed SST anomaly onto (c) the principal component of SON (solid line) and DJF (dashed line) EOF at 0.05 ℃ intervals. SST anomalies greater (less) than 0.05 (-0.05) ℃ are lightly (heavily) shaded. The bars in the lower panel show the normalized NINO3 calculated from the SON mean data.

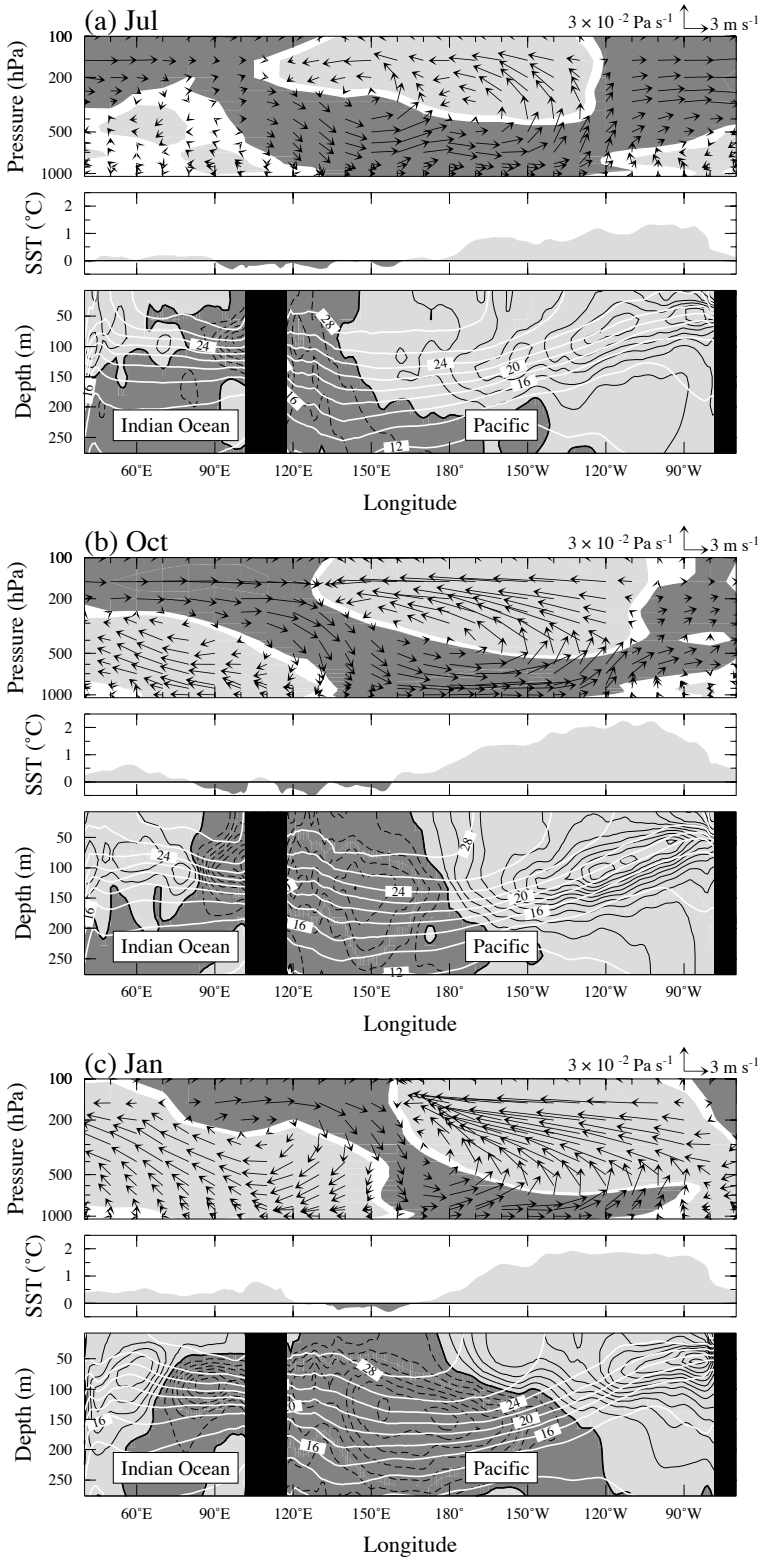

FIG. 5. The vertical section of the composite anomalies of zonal and vertical wind velocity (top), SST (middle), and subsurface temperature (bottom) in (a) July, (b) October and (c) the following January for the coincidence years (1963, 72, 80, 86, 97). Each of variables is averaged over the equatorial region between 5°S and 5°N. The zonal wind anomalies greater (less) than 0.2 (-0.2) m s^{-1}in the top panel are heavily (lightly) shaded. The positive (negative) SST and subsurface temperature are lightly (heavily) shaded in the middle and bottom panels, respectively. The white and black contours in the bottom panel show the climatology (contour interval: 2 ℃) and anomaly (contour interval: 0.4 ℃) of temperature in the upper-ocean.

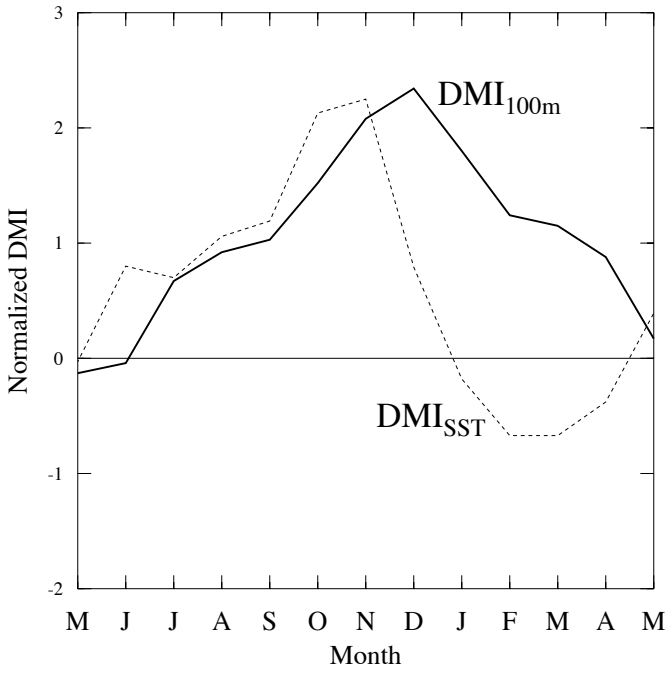

FIG. 6. The monthly composite Dipole Mode Indices (DMIs) defined at the surface (dashed line) and 100m-depth (solid line) for the coincidence years (1963, 72, 82, 86, 97). Each of the indices is normalized.

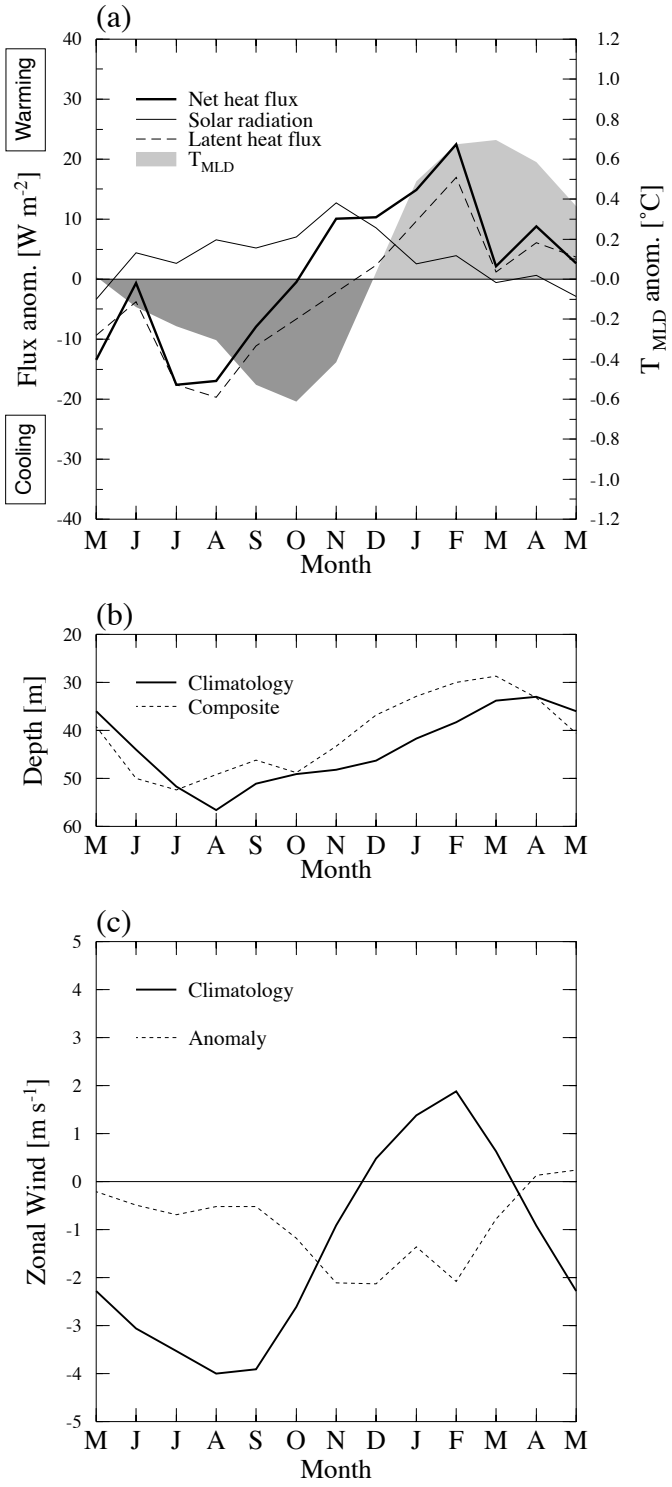

FIG. 7. The monthly composite anomalies of (a) surface latent heat (dashed line), solar radiation (thin line), total net heat flux (thick line), and mixed layer temperature (shaded) averaged over the eastern Indian Ocean (90 ˚- 110 ˚E, 10 ˚S - 0 ˚) for the coincidence years (1963, 72, 82, 86, 97). The positive (negative) value of surface heat fluxes means downward (upward) flux anomaly. (b) and (c) are the same as in (a), but for (b) the mixed layer depth (climatology: solid line, composite: dotted line) and (c) the surface zonal wind (climatology: solid line, anomaly: dotted line), respectively.

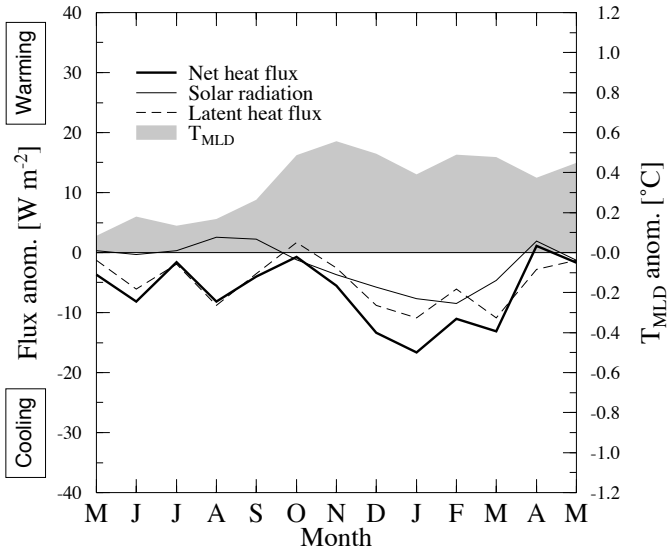

FIG. 8. Same as in Fig. 7a, but for the monthly composite anomalies averaged over the western Indian Ocean (50 ˚- 70 ˚E, 10 ˚S - 10 ˚N).